Abnormalities in aortic properties: a potential link between left ventricular diastolic function and ventricular-aortic coupling in sickle cell disease

Emilie Bollache, Nadjia Kachenoura, Roberto Lang, Ankit Desai, Victor Mor-Avi, Amit Patel

Abnormalities in Aortic Properties: A Potential Link Between Left Ventricular Diastolic Function and Ventricular – Aortic Coupling in Sickle Cell Disease

Emilie Bollache PhD[1], Nadjia Kachenoura PhD[1], Roberto M. Lang MD[2],

Ankit A. Desai MD[3], Victor Mor-Avi PhD[2], Amit R. Patel MD[2]

[1]Sorbonne Universités, UPMC Univ Paris 06, INSERM 1146, CNRS 7371, Laboratoire d'Imagerie Biomédicale, 75013 Paris, France

[2]Department of Medicine, University of Chicago Medical Center, Chicago, Illinois, USA

[3]Department of Medicine, University of Arizona, Tucson, Arizona, USA

Short title: **Aortic Abnormalities in Sickle Cell Disease**

Correspondence to:

Victor Mor-Avi, Ph.D.

University of Chicago

5841 S. Maryland Ave., MC5084

Chicago, Illinois 60637, USA

Tel: 773.702.7780

Fax: 773.834.1034

E-mail: vmoravi@bsd.uchicago.edu

Abstract

Background. Left ventricular (LV) diastolic dysfunction in patients with sickle cell disease (SCD) is associated with increased mortality. However, its mechanisms are not well known, preventing the development of effective therapies. We hypothesized that patients with SCD have altered aortic properties despite normal blood pressure, which may contribute towards the development of diastolic dysfunction. **Methods.** We studied 31 stable adult patients with SCD (32±7 yrs) and 12 healthy controls of similar age (29±10 yrs) who underwent echocardiography and cardiovascular magnetic resonance (CMR) imaging on the same day. Echocardiographic measurements of mitral inflow and mitral annulus velocities were used to evaluate LV diastolic function. CMR imaging included standard LV function evaluation and myocardial tissue characterization as well as velocity-encoded images of the ascending aorta to measure aortic diastolic cross-sectional area, distensibility, as well as peaks and volumes of the global, forward and backward blood flow rate. **Results.** Compared to controls, SCD patients had increased aortic diastolic area, global stroke volume, and both forward and backward flow, while aortic distensibility and peripheral blood pressure were similar. Furthermore, peak backward flow rate and volume were able to discriminate between patients with and without diastolic dysfunction. **Conclusions.** Our findings show that some aortic properties are altered in SCD patients and may be associated with diastolic dysfunction despite normal systolic blood pressure. If confirmed in larger studies, these aortic changes could be a novel therapeutic target to prevent or delay the development of LV diastolic dysfunction in SCD and thus potentially improve outcomes in these patients.

Introduction

Sickle cell disease (SCD), which is a group of inherited blood disorders characterized by red blood cells that assume an abnormal, rigid, sickle shape and contain abnormal hemoglobin, is one of the most common genetic diseases worldwide and an important cause of morbidity and mortality[1]. SCD is associated with anemia, small vessel occlusion and tissue ischemia[1], which can occur in different organs including the heart[2], as well as progressive vasculopathies, including pulmonary hypertension[3] and peripheral arterial endothelial dysfunction[4].

Left ventricular (LV) alterations in SCD have been widely described, including LV dilation[4–13], an increase in LV mass[5,7,14,4,8,10–13], as well as diastolic dysfunction[7,11,13,15]. Today, up to 25% of SCD deaths are related to cardiovascular causes[16] and diastolic dysfunction is a known independent risk factor for mortality in SCD patients[17]. However, the etiology of LV diastolic dysfunction in SCD remains unclear, preventing the development of effective therapies. In fact, previous work published by our group has suggested that the development of diastolic dysfunction in SCD may be independent of mechanisms such as myocardial iron overload, fibrosis, and abnormal microvascular perfusion[12].

Several studies have focused on the effects of SCD on large central arteries, based on aortic size[4–6] or arterial stiffness[4,12,14,18,19]. In these studies, arterial stiffness was found to be related to indexed LV mass[4,14] and indices of LV diastolic dysfunction[4,12]. However, other potential determinants of LV diastolic dysfunction, such as proximal aortic blood flow hemodynamics, have never been investigated in SCD patients. Indeed, the only previously reported hemodynamics indices were either cardiac output[9,18,19] or blood flow measured in peripheral arteries[20–22]. We hypothesized that patients with SCD have abnormalities in aortic properties despite the presence of normal blood pressure, which may contribute towards the development of diastolic dysfunction.

Accordingly, our aims were: 1) to perform a comprehensive evaluation of SCD-related changes in aortic size and function, and 2) to study the interaction between changes in the aorta and LV diastolic function. To achieve these aims, we used a multimodality approach that involved echocardiography and cardiovascular magnetic resonance (CMR) imaging, providing a thorough evaluation of LV systolic and diastolic function, myocardial tissue characteristics, as well as size, stiffness and blood flow patterns in the ascending aorta.

Materials and methods

Study group

Subjects from the University of Chicago Medical Center were recruited from the adult SCD outpatient program. Details of trial registration are provided at the following website: http://clinicaltrials.gov/ct2/show/NCT01044901. A total of 31 clinically stable African-American patients with SCD (including individuals with hemoglobin SS, SC, and β-thalassemia demonstrated by high-performance liquid chromatographic separation or gel electrophoresis) and 12 healthy subjects of a similar age were enrolled in this study. Each subject underwent transthoracic echocardiography (TTE) and CMR imaging within 4 hours. Subjects were excluded if they were clinically unstable, defined as having vaso-occlusive crisis, acute chest syndrome or unscheduled blood transfusions within 3 weeks of the study, or had standard contra-indications to CMR. Each subject provided written informed consent to participate in this study, which was approved by the Institutional Review Board.

Echocardiography

TTE images were obtained using an iE33 ultrasound imaging system with an S5 transducer (Philips Healthcare, Andover, MA). Digital cine loops were acquired by a single experienced sonographer and subsequently reviewed off line following current guidelines[23], to measure

left atrial volume, transmitral flow early filling and atrial filling peak velocities (E and A, respectively), as well as mitral annular early peak longitudinal velocity on the septal and lateral walls (e') from tissue Doppler imaging. These parameters were used to diagnose LV diastolic dysfunction, according to the current guidelines of the American Society of Echocardiography[24].

Acquisition of CMR data

CMR imaging was performed using a 1.5 T scanner (Achieva, Philips, Best, Netherlands) with a 5-element phased array cardiac coil. It included assessments of myocardial and hepatic iron, cardiac function, replacement myocardial fibrosis, as well as acquisition of velocity-encoded data in the ascending aorta.

First, to assess for myocardial iron deposition, T2* imaging using a single breath-hold, black-blood multi echo (2.3 to 14 msec) cardiac-triggered spin echo pulse sequence was performed in one mid-ventricular short axis slice and one coronal slice through the liver to assess myocardial and hepatic iron content, respectively. Then, to assess cardiac function, retrospectively gated cine images were acquired using a steady-state free precession (SSFP) sequence with the following acquisition parameters: repetition time (TR) = 2.9 msec, echo time (TE) = 1.5 msec, flip angle = 60°, acquisition matrix = 192x168, pixel spacing = 1.3 mm and temporal resolution < 40 msec. Standard long-axis including four-chamber, two-chamber, and three-chamber views, as well as short-axis slices (thickness = 8 mm, gap = 2 mm) covering the entire heart were obtained. Subsequently, to assess for myocardial fibrosis, late gadolinium enhancement (LGE) images were further acquired in the aforementioned short- and long-axis views, 10 minutes after the administration of 0.15 mmol/kg of gadolinium-DTPA-BMA (Omniscan[TM]) using a T1-weighted gradient echo pulse sequence with a phase sensitive inversion recovery reconstruction (TR = 4.5 msec, TE = 2.2 msec, inversion time = 250-300 msec, voxel size = 2x2x10 mm^3, SENSE factor = 2). An inversion time typically

between 250 and 300 msec was used to achieve nulling of normal myocardium. Finally, axial phase-contrast images were acquired in the mid-ascending aorta perpendicular to the aorta at the level of the center of the right pulmonary artery, using a 2D through-plane velocity-encoded sequence with retrospective gating during breath-holding. Typical acquisition parameters were: TR = 4.2 msec, TE = 2.6 msec, flip angle = 15°, number of excitation = 1, voxel size = 1.4x1.4x10 mm^3, acquisition matrix = 140x133, temporal resolution = 29 msec and encoding velocity = 200 cm/sec. The aorta was always at the centre of the acquired image to minimize background offset effects. Heart rate, blood pressure, and symptoms were monitored throughout the entire examination.

Analysis of CMR data

T2*, SSFP and LGE images were analyzed using commercial software (Philips ViewForum, Best, Netherlands). First, tissue T2* signal intensity was measured in a homogenous region of interest in the LV septum and in the liver at two separate echo times (TE): T2* = - ΔTE/ln (SI$_{TE2}$/ SI$_{TE1}$), where ΔTE represents the time difference between the two echo times and SI$_{TE1}$ and SI$_{TE2}$ represent signal intensity at these echo times. Then, SSFP short-axis images were used to measure LV end-diastolic and end-systolic volumes, mass, and ejection fraction by the Simpson method of disks[25]. All volumes and mass were indexed for body surface area (BSA). Finally, LGE was considered to be present in the LV myocardium if the signal intensity was above 5 x standard deviations of the mean signal intensity of a remote normal myocardial segment and if it was seen in 2 adjacent slices or transverse imaging planes.

Analysis of aortic CMR data

Each aortic phase-contrast CMR dataset contained both modulus anatomical and velocity images throughout the cardiac cycle, which were processed using previously validated software (ArtFun, U1146 Inserm / UPMC)[26]. First, ascending aorta contours were automatically segmented on each phase of the cardiac cycle on modulus images, resulting in

aortic lumen area variations throughout the cardiac cycle (**Figure 1A**). Furthermore, superimposition of the aortic contours on velocity images provided aortic flow variations (**Figure 1B**). Temporal curves were then processed using automated peak detection and area under curve calculation.

First, ascending aorta diastolic (A_D) and systolic (A_S) areas (cm²) were calculated, respectively as the minimum and maximum of the aforementioned cross-sectional area variation curve. The stiffness-related aortic distensibility was then estimated as: $(A_S - A_D) / (A_D \times PP)$, where PP is the pulse pressure (mmHg) calculated as the difference between systolic and diastolic brachial blood pressures recorded during the CMR exam[27]. A_D indexed for BSA was also reported.

Then, ascending aortic flow rate curves were used to estimate aortic global flow peak (ml/sec) and stroke volume (ml). Global net flow (V_N) and regurgitant (V_R) volumes were also calculated to measure aortic regurgitation fraction as $100 * V_R / V_N$ (%). We further studied the separate contributions of forward and backward flow components to the global flow by using the CMR velocity data[28]. To this effect, for each velocity-encoded image collected during the cardiac cycle, pixels corresponding to the velocities encoded in the direction of blood flow ejected from the left ventricle ('positive' pixels) were used to calculate forward flow, while pixels corresponding to the velocities encoded in the direction opposite to the ejected flow ('negative' pixels) were used to calculate backward flow (**Figure 1B**). Then, aortic forward and backward flow curves throughout the cardiac cycle were used to compute, respectively:

1) peak forward flow rate (ml/sec) and volume (ml),

2) peak backward flow rate (ml/sec) and volume (ml) as well as its onset time (msec) .

All peak flow rate and volume indices were normalized by BSA. Finally, ratios of backward to peaks forward flow and volumes were computed.

Statistical analysis

Mean values and standard deviations (SD) were provided for continuous variables. For comparison of baseline characteristics, TTE and CMR indices of LV function as well as CMR parameters of aortic geometry, stiffness and flow between SCD patients and healthy controls, a nonparametric Mann–Whitney test was used. Differences in aortic indices between SCD patients with and without LV diastolic dysfunction were illustrated using box plots and statistical significance was studied using a Mann–Whitney test. All reported p-values are two-sided and a p-value <0.05 indicated statistical significance. Statistical analysis was performed using Stata 10 IC (StataCorp LP, College Station, Texas, USA).

Results

Healthy subjects' and SCD patients' baseline characteristics along with TTE and CMR indices of LV function are summarized in **Table 1**. Age, gender distribution, and body surface area did not differ between the two groups. There was also no difference in blood pressure between the two groups. While LV ejection fraction was similar, indexed LV volumes and mass were significantly increased in SCD patients, as compared to controls. LGE was noted in 5 SCD patients, indicating myocardial fibrosis. Liver T2* was significantly decreased in SCD patients, indicating hepatic iron overload, whereas only one patient had a reduced myocardial T2*, indicating myocardial iron overload. Regarding LV diastolic function, E and A velocities were significantly increased in SCD patients when compared to controls; however the observed decrease in E/A ratio was not statistically significant. Finally, septal and lateral mitral annulus velocities, e', were reduced in SCD patients, resulting in a significant increase in E/e' ratio. Diastolic dysfunction was found in 5 (16%) patients with

SCD, and was classified as Grade 2 in all of them. None of these 5 patients had either myocardial fibrosis or iron overload.

Aortic changes in SCD patients

Table 2 summarizes CMR indices of aortic geometry, stiffness and hemodynamics for SCD patients and controls. While no significant differences in ascending aortic distensibility were found between these two groups, aortic area global peak flow rate and stroke volume were significantly higher in SCD patients when compared to controls. When looking at separate contributions of forward and backward flow, we found that both components were significantly elevated in SCD patients, in terms of peak flows and volumes.

Associations of aortic indices with LV diastolic function

In the SCD group, the aforementioned differences in aortic indices were even more prominent in patients with diastolic dysfunction (age: 35±8 years), when compared to patients with normal diastolic function (age: 31±7 years, p=0.22 vs. patients with diastolic dysfunction), and were significant for backward flow indices (**Figures 2 and 3**). Of note, aortic distensibility was considerably reduced in patients with diastolic dysfunction, although this difference was not statistically significant.

Discussion

In this multimodality imaging study involving echocardiography and CMR imaging, we found differences in aortic geometry and hemodynamics between SCD patients and normal controls despite the absence of differences in age or blood pressure. We also found that SCD-related changes were more pronounced in the presence of diastolic dysfunction. Our main findings were that: 1) the proximal aorta was dilated with all global, forward and backward flow components were increased without elasticity changes in SCD patients, as compared to

controls, 2) indices of aortic backward flow volumes were able to discriminate between SCD patients with and without diastolic dysfunction.

Cardiac alterations in SCD have been previously studied. In agreement with published literature, we found in our SCD patients a preserved LV ejection fraction[5,19,8,11,13] along with LV dilation[5–7,4,8,10,11,13] and an increase in LV mass[5–7,14,4,8,10,11,13]. Such LV enlargement has been hypothesized to reflect a remodeling mechanism to adapt to the elevation in stroke volume induced by the chronic anemia-related decrease in blood oxygenation in such disease to match metabolic demand[29]. Consistently, we observed in SCD patients an elevation in stroke volume measured in the ascending aorta from velocity-encoded CMR data.

Previous studies focusing on the dilating and stiffening effects of SCD on large central arteries resulted in conflicting findings. Indeed, investigators have not only shown that aortic size was paradoxically unchanged[4] or increased[5,6], but also that arterial stiffness was either decreased[30] or increased[4,14,31] in SCD patients. In the current study, we found that aortic area was significantly increased and that central aortic stiffness was unchanged in SCD patients when compared to controls. These discrepancies might be due to differences in study populations as well as in techniques and specific arterial beds used to measure arterial stiffness. Indeed, we calculated local distensibility in the proximal ascending aorta while in most previous studies [12,14,30,31], arterial stiffness was assessed from measurements performed in the carotid, brachial, radial and femoral arteries. Furthermore, the previously used stiffness-related brachio-radial[14], carotid-radial[30] or carotid-femoral[30] pulse wave velocities measure global distensibility, since they include arterial segments that have different elasticity, and therefore do not always reflect central aortic elasticity, which is known to decrease towards peripheral arteries[32]. However, we found that distensibility was highly decreased in SCD patients with LV diastolic dysfunction, when compared to those with a normal diastolic

function. This difference was not statistically significant, likely reflecting the relatively small sample size.

We further evaluated SCD-related changes in aortic hemodynamics, while studying separately the forward and backward flow components obtained from CMR velocity-encoded data. Indeed, aortic blood flow includes a forward (=antegrade) flow originating from the left ventricle and going through the aorta, and a backward (=reverse) flow, reflecting back to the heart from branching sites and affected by differences in aortic geometry. This general physiological phenomenon has been described in the literature previously[33]; it can be amplified in case of various cardiovascular diseases such as aortic aneurysms[34] or ischemic heart disease[35], but it is always present even in healthy subjects. In a recent study[28] including 96 healthy subjects, it was observed that such backward flow increased in terms of peak flow rate and volume with aging, and that it appeared earlier in the cardiac cycle. It was also shown that aortic geometry, namely aortic cross-sectional dilation and aortic arch elongation, was the major determinant of backward flow. Thus, backward flow might mostly represent local flow disorganization due to aortic geometric changes. In our SCD patients, we found that aortic dilation was accompanied by increased backward flow peak and volume when compared to healthy subjects.

Importantly, indices of backward flow volume were significantly higher in SCD patients with diastolic dysfunction when compared to those with a normal diastolic function. Thus, chronic anemia in SCD might induce an increase in stroke volume, which in turn may result in aortic dilatation along with an increase in aortic backward flow. This increased afterload may ultimately lead to a further impairment of LV diastolic function.

Our study has several limitations. First, we calculated aortic distensibility using brachial blood pressure rather than central pressure, which could have confounded potential changes in

the true proximal aortic local stiffness. Also, the cross-sectional feature of our study does not allow identifying causes and effects involved in the changes in LV-aortic interactions in SCD. Finally, this is a small, single center study and the findings need to be confirmed in a larger SCD patient population, that would allow multiple regression analysis to identify factors associated with diastolic dysfunction. Importantly, however, in our previous study, we found no association between diastolic dysfunction and myocardial fibrosis, myocardial iron overload or microvascular dysfunction [12].

Despite these limitations, we found a significant increase in ascending aortic area, as well as alterations in global, forward and backward flow peak velocities and volumes in SCD patients. These differences were noted even though peripheral arterial blood pressure was normal. This finding underscores the importance of the search for new diagnostic markers of aortic function, because LV diastolic dysfunction is not associated with hypertension in these patients. Interestingly, in our study, the elevation in backward flow was even more pronounced in patients with diastolic dysfunction. If confirmed in larger and longitudinal studies, these aortic changes could become useful as they may allow an early detection of LV diastolic dysfunction and could ultimately be targets for specific therapies, as a way to prevent or delay the development of diastolic dysfunction in SCD and thus potentially improve outcomes in this patient population.

Disclosures: None of the authors have any potential conflicts of interest to disclose.

References

1. Rees DC, Williams TN, Gladwin MT. Sickle-cell disease. Lancet. 2010; 376:2018–2031.

2. Acar P, Maunoury C, de Montalembert M, Dulac Y. [Abnormalities of myocardial perfusion in sickle cell disease in childhood: a study of myocardial scintigraphy]. Arch Mal Coeur Vaiss. 2003; 96:507–510.

3. Sutton LL, Castro O, Cross DJ, Spencer JE, Lewis JF. Pulmonary hypertension in sickle cell disease. Am J Cardiol. 1994; 74:626–628.

4. Aessopos A, Farmakis D, Tsironi M, Diamanti-Kandarakis E, Matzourani M, Fragodimiri C, Hatziliami A, Karagiorga M. Endothelial function and arterial stiffness in sickle-thalassemia patients. Atherosclerosis. 2007; 191:427–432.

5. Gerry JL, Baird MG, Fortuin NJ. Evaluation of left ventricular function in patients with sickle cell anemia. Am J Med. 1976; 60:968–972.

6. Covitz W, Espeland M, Gallagher D, Hellenbrand W, Leff S, Talner N. The heart in sickle cell anemia. The Cooperative Study of Sickle Cell Disease (CSSCD). Chest. 1995; 108:1214–1219.

7. Şan M, Demirtaş M, Burgut R, Birand A, Başlamişh F. Left Ventricular Systolic and Diastolic Functions in Patients With Sickle Cell Anemia. Int J Angiol Off Publ Int Coll Angiol Inc. 1998; 7:185–187.

8. Westwood MA, Shah F, Anderson LJ, Strange JW, Tanner MA, Maceira AM, Howard J, Porter JB, Walker JM, Wonke B, Pennell DJ. Myocardial tissue characterization and the role of chronic anemia in sickle cell cardiomyopathy. J Magn Reson Imaging JMRI. 2007; 26:564–568.

9. Voskaridou E, Christoulas D, Terpos E. Sickle-cell disease and the heart: review of the current literature. Br J Haematol. 2012; 157:664–673.

10. Junqueira FP, Fernandes JL, Cunha GM, T A Kubo T, M A O Lima C, B P Lima D, Uellendhal M, Sales SR, A S Cunha C, L R de Pessoa V, L C Lobo C, Marchiori E. Right and left ventricular function and myocardial scarring in adult patients with sickle cell disease: a comprehensive magnetic resonance assessment of hepatic and myocardial iron overload. J Cardiovasc Magn Reson Off J Soc Cardiovasc Magn Reson. 2013; 15:83.

11. Barbosa MM, Vasconcelos MCM, Ferrari TCA, Fernandes BM, Passaglia LG, Silva CM, Nunes MCP. Assessment of ventricular function in adults with sickle cell disease: role of two-dimensional speckle-tracking strain. J Am Soc Echocardiogr Off Publ Am Soc Echocardiogr. 2014; 27:1216–1222.

12. Desai AA, Patel AR, Ahmad H, Groth JV, Thiruvoipati T, Turner K, Yodwut C, Czobor P, Artz N, Machado RF, Garcia JGN, Lang RM. Mechanistic insights and characterization of sickle cell disease-associated cardiomyopathy. Circ Cardiovasc Imaging. 2014; 7:430–437.

13. Hammoudi N, Arangalage D, Djebbar M, Stojanovic KS, Charbonnier M, Isnard R, Girot R, Michel P-L, Lionnet F. Subclinical left ventricular systolic impairment in steady state young adult patients with sickle-cell anemia. Int J Cardiovasc Imaging. 2014; 30:1297–1304.

14. Cheung YF, Chan GCF, Ha SY. Arterial stiffness and endothelial function in patients with beta-thalassemia major. Circulation. 2002; 106:2561–2566.

15. Ahmad H, Gayat E, Yodwut C, Abduch MC, Patel AR, Weinert L, Desai A, Tsang W, Garcia JGN, Lang RM, Mor-Avi V. Evaluation of myocardial deformation in patients with sickle cell disease and preserved ejection fraction using three-dimensional speckle tracking echocardiography. Echocardiogr. 2012; 29:962–969.

16. Fitzhugh CD, Lauder N, Jonassaint JC, Telen MJ, Zhao X, Wright EC, Gilliam FR, De Castro LM. Cardiopulmonary complications leading to premature deaths in adult patients with sickle cell disease. Am J Hematol. 2010; 85:36–40.

17. Sachdev V, Machado RF, Shizukuda Y, Rao YN, Sidenko S, Ernst I, St Peter M, Coles WA, Rosing DR, Blackwelder WC, Castro O, Kato GJ, Gladwin MT. Diastolic dysfunction is an independent risk factor for death in patients with sickle cell disease. J Am Coll Cardiol. 2007; 49:472–479.

18. Varat MA, Adolph RJ, Fowler NO. Cardiovascular effects of anemia. Am Heart J. 1972; 83:415–426.

19. Denenberg BS, Criner G, Jones R, Spann JF. Cardiac function in sickle cell anemia. Am J Cardiol. 1983; 51:1674–1678.

20. Hatch FE, Crowe LR, Miles DE, Young JP, Portner ME. Altered vascular reactivity in sickle hemoglobinopathy. A possible protective factor from hypertension. Am J Hypertens. 1989; 2:2–8.

21. Belhassen L, Pelle G, Sediame S, Bachir D, Carville C, Bucherer C, Lacombe C, Galacteros F, Adnot S. Endothelial dysfunction in patients with sickle cell disease is related to selective impairment of shear stress-mediated vasodilation. Blood. 2001; 97:1584–1589.

22. Eberhardt RT, McMahon L, Duffy SJ, Steinberg MH, Perrine SP, Loscalzo J, Coffman JD, Vita JA. Sickle cell anemia is associated with reduced nitric oxide bioactivity in peripheral conduit and resistance vessels. Am J Hematol. 2003; 74:104–111.

23. Lang RM, Badano LP, Mor-Avi V, Afilalo J, Armstrong A, Ernande L, Flachskampf FA, Foster E, Goldstein SA, Kuznetsova T, Lancellotti P, Muraru D, Picard MH, Rietzschel ER, Rudski L, Spencer KT, Tsang W, Voigt J-U. Recommendations for cardiac chamber quantification by echocardiography in adults: an update from the American Society of Echocardiography and the European Association of Cardiovascular Imaging. J Am Soc Echocardiogr Off Publ Am Soc Echocardiogr. 2015; 28:1–39.e14.

24. Nagueh SF, Appleton CP, Gillebert TC, Marino PN, Oh JK, Smiseth OA, Waggoner AD, Flachskampf FA, Pellikka PA, Evangelisa A. Recommendations for the evaluation of left

ventricular diastolic function by echocardiography. Eur J Echocardiogr J Work Group Echocardiogr Eur Soc Cardiol. 2009; 10:165–193.

25. Lorenz CH, Walker ES, Morgan VL, Klein SS, Graham TP. Normal human right and left ventricular mass, systolic function, and gender differences by cine magnetic resonance imaging. J Cardiovasc Magn Reson Off J Soc Cardiovasc Magn Reson. 1999; 1:7–21.

26. Herment A, Kachenoura N, Lefort M, Bensalah M, Dogui A, Frouin F, Mousseaux E, De Cesare A. Automated segmentation of the aorta from phase contrast MR images: validation against expert tracing in healthy volunteers and in patients with a dilated aorta. J Magn Reson Imaging JMRI. 2010; 31:881–888.

27. Dogui A, Kachenoura N, Frouin F, Lefort M, De Cesare A, Mousseaux E, Herment A. Consistency of aortic distensibility and pulse wave velocity estimates with respect to the Bramwell-Hill theoretical model: a cardiovascular magnetic resonance study. J Cardiovasc Magn Reson Off J Soc Cardiovasc Magn Reson. 2011; 13:11.

28. Bensalah MZ, Bollache E, Kachenoura N, Giron A, De Cesare A, Macron L, Lefort M, Redheuill A, Mousseaux E. Geometry is a major determinant of flow reversal in proximal aorta. Am J Physiol Heart Circ Physiol. 2014; 306:H1408–1416.

29. Gladwin MT, Sachdev V. Cardiovascular abnormalities in sickle cell disease. J Am Coll Cardiol. 2012; 59:1123–1133.

30. Lemogoum D, Van Bortel L, Najem B, Dzudie A, Teutcha C, Madu E, Leeman M, Degaute J-P, van de Borne P. Arterial stiffness and wave reflections in patients with sickle cell disease. Hypertension. 2004; 44:924–929.

31. Belizna C, Loufrani L, Ghali A, Lahary A, Primard E, Louvel J-P, Henrion D, Lévesque H, Ifrah N. Arterial stiffness and stroke in sickle cell disease. Stroke J Cereb Circ. 2012; 43:1129–1130.

32. Latham RD, Westerhof N, Sipkema P, Rubal BJ, Reuderink P, Murgo JP. Regional wave travel and reflections along the human aorta: a study with six simultaneous micromanometric pressures. Circulation. 1985; 72:1257–1269.

33. Bogren HG, Klipstein RH, Firmin DN, Mohiaddin RH, Underwood SR, Rees RS, Longmore DB. Quantitation of antegrade and retrograde blood flow in the human aorta by magnetic resonance velocity mapping. Am Heart J. 1989; 117:1214–1222.

34. Hope TA, Markl M, Wigström L, Alley MT, Miller DC, Herfkens RJ. Comparison of flow patterns in ascending aortic aneurysms and volunteers using four-dimensional magnetic resonance velocity mapping. J Magn Reson Imaging JMRI. 2007; 26:1471–1479.

35. Bogren HG, Mohiaddin RH, Klipstein RK, Firmin DN, Underwood RS, Rees SR, Longmore DB. The function of the aorta in ischemic heart disease: a magnetic resonance and angiographic study of aortic compliance and blood flow patterns. Am Heart J. 1989; 118:234–247.

Figures

Figure 1. A. Segmentation (left, white contours) of ascending aortic borders showed on several systolic phase-contrast modulus CMR images, used for the estimation of aortic cross-sectional area variations throughout the cardiac cycle (right). B. Superimposition of ascending aortic borders (left, white contours) on the simultaneous systolic velocity images used for the estimation of aortic global, forward and backward flow variations throughout the cardiac cycle (right). Positive velocities pertaining to forward flow are color-coded in hot tones while negative velocities pertaining to backward flow are color-coded in cold tones.
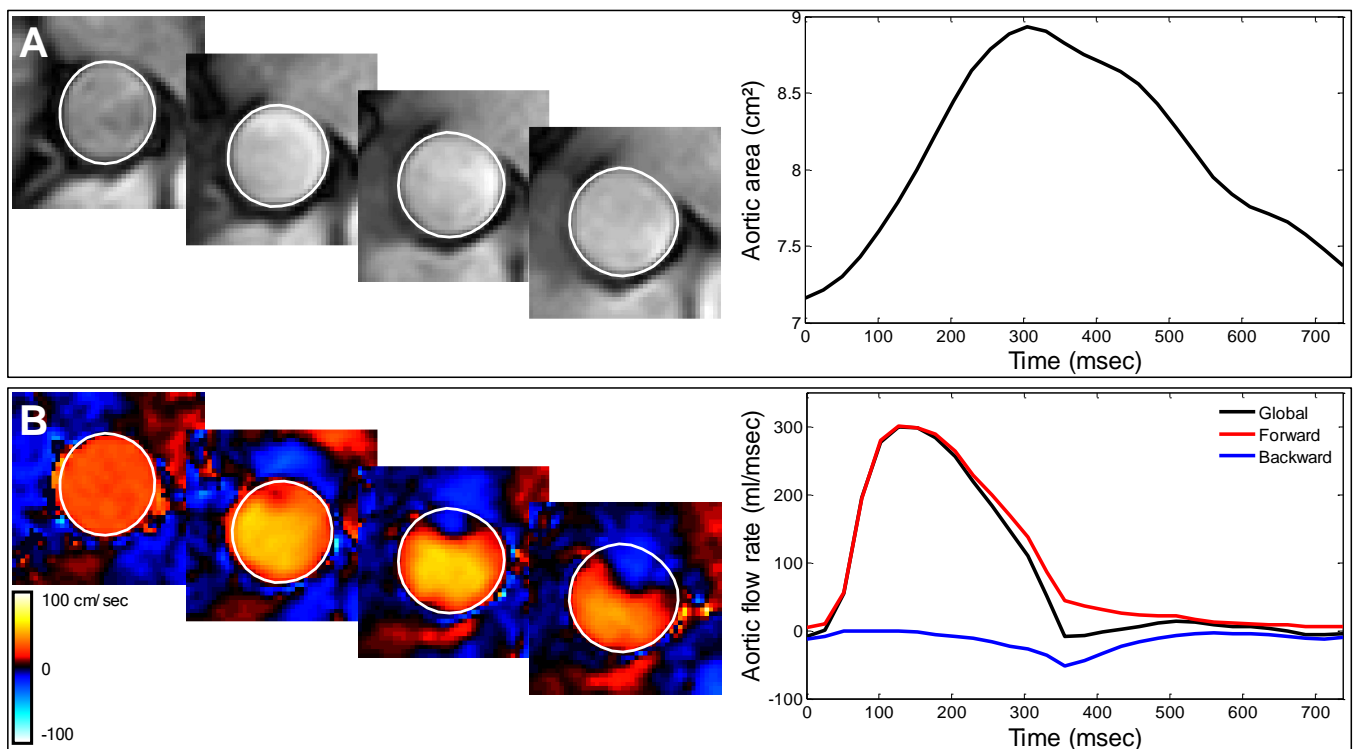
Figure 2. Box plots of indices of aortic geometry and stiffness in SCD patients without and with diastolic dysfunction. Horizontal solid lines represent median values while dashed lines represent first and third quartiles.

Figure 3. Box plots of indices of aortic hemodynamics in SCD patients without and with diastolic dysfunction. Horizontal solid lines represent median values while dashed lines represent first and third quartiles. * p<0.05.
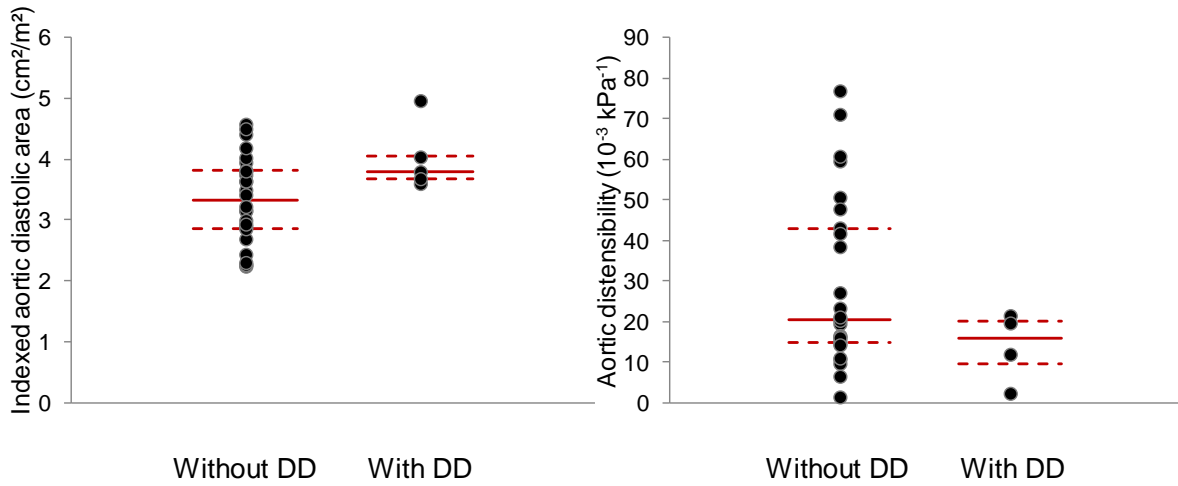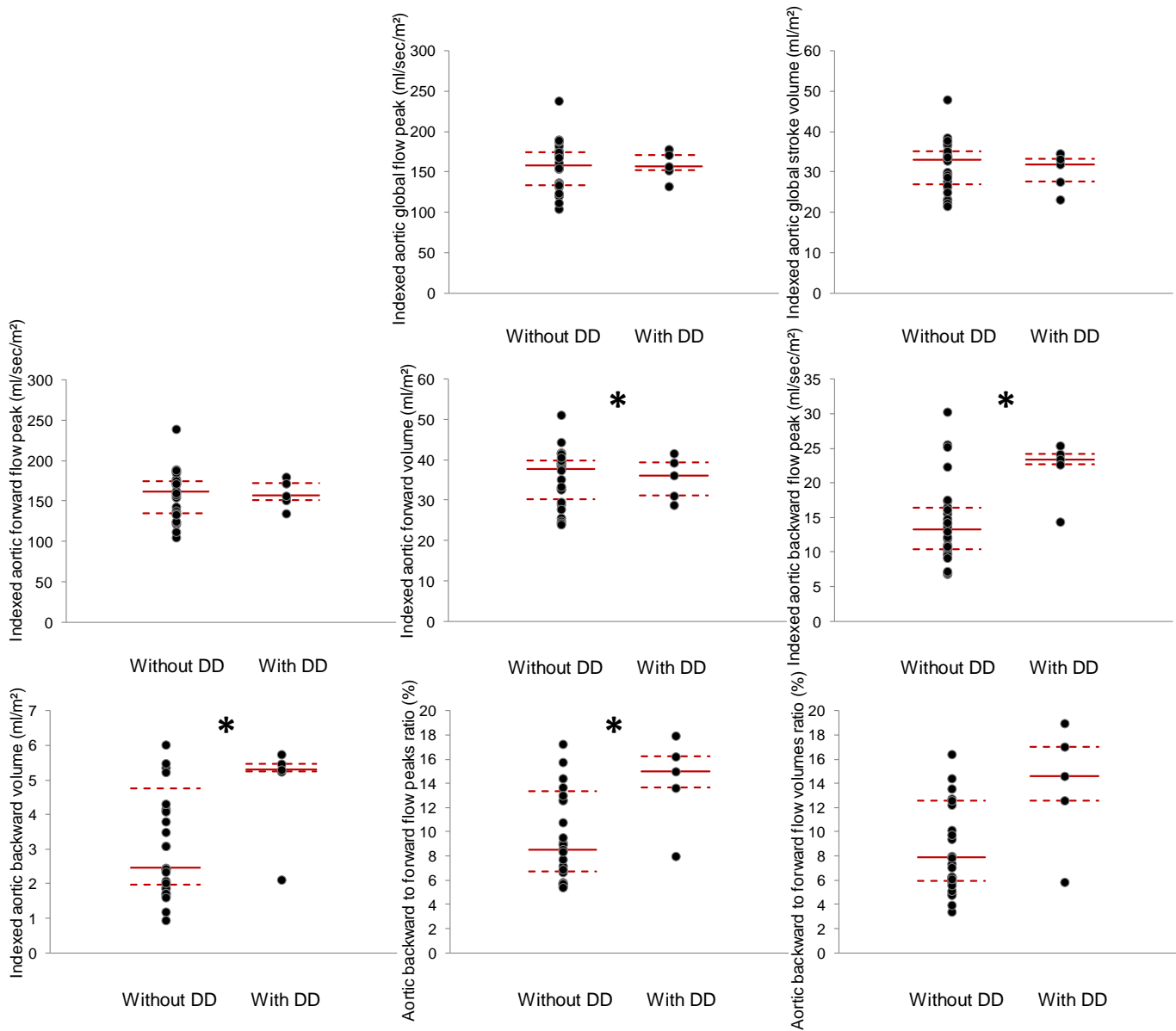
Table 1 – Baseline characteristics as well as CMR and TTE indices of LV function and iron overload for healthy subjects and patients with SCD.

	Healthy subjects (*n*=12)	SCD patients (*n*=31)
Baseline characteristics		
Age, years	29 ± 10	32 ± 7
Gender, females *n* (%)	7 (58)	18 (58)
Body surface area, m²	1.92 ± 0.30	1.80 ± 0.19
Heart rate, bpm	74 ± 14	70 ± 15
Systolic blood pressure, mmHg	125 ± 19	121 ± 20
Diastolic blood pressure, mmHg	71 ± 12	66 ± 18
Hemoglobin level, g/dL	-	8.5 ± 2.5
CMR indices		
LV ejection fraction, %	62 ± 5.9	58 ± 5.0
Indexed LV end-diastolic volume, ml/m²	79 ± 12	123 ± 28[†††]
Indexed LV end-systolic volume, ml/m²	31 ± 7.2	53 ± 15[†††]
Indexed LV mass, g/m²	50 ± 13	78 ± 20[††]
Presence of LGE, *n* (%)	-	5 (16)
Myocardial T2*, msec	35 ± 7.7	42 ± 12[†]
Liver T2*, msec	32 ± 9.5	16 ± 12[††]
TTE indices of LV diastolic function		
E velocity, cm/sec	85 ± 13	97 ± 15[†]
A velocity, cm/sec	51 ± 21	60 ± 16[†]
E/A ratio	1.9 ± 0.6	1.7 ± 0.5
Septal e', cm/sec	10.6 ± 1.9	9.1 ± 1.4[†]
Lateral e', cm/sec	14.5 ± 3.2	13.3 ± 3.2
E/e'$_{sept}$ ratio	8.2 ± 1.5	10.8 ± 2.3[††]
E/e'$_{lat}$ ratio	6.1 ± 2.0	7.6 ± 2.2[†]
Indexed left atrial volume, ml/m²	41 ± 9	66 ± 17[†††]

[†]: $p<0.05$
[††]: $p<0.005$
[†††]: $p<0.0001$

Table 2 – CMR indices of aortic geometry, stiffness and hemodynamics for healthy subjects and patients with SCD.

	Healthy subjects (*n*=12)	SCD patients (*n*=31)
Geometry		
Indexed aortic diastolic area, cm²/m²	2.7 ± 0.3	3.4 ± 0.7**
Stiffness		
Aortic distensibility, 10^{-3} kPa^{-1}	24 ± 15	27 ± 20
Hemodynamics		
Indexed aortic global flow rate peak, ml/sec/m²	120 ± 22	157 ± 28**
Indexed aortic stroke volume, ml/m²	22 ± 3.9	31 ± 5.9***
Aortic regurgitation fraction, %	1.0 ± 0.6	1.2 ± 1.2
Indexed aortic forward flow rate peak, ml/sec/m²	120 ± 22	158 ± 28**
Indexed aortic forward flow volume, ml/m²	25 ± 4.3	36 ± 6.6***
Indexed aortic backward flow rate peak, ml/sec/m²	11 ± 2.2	16 ± 6.4*
Indexed aortic backward flow volume, ml/m²	2.0 ± 0.9	3.3 ± 1.6*
Aortic backward flow appearance time, msec	261 ± 20	277 ± 29*
Aortic backward to forward flow peaks ratio, %	9.1 ± 2.2	10.0 ± 4.0
Aortic backward to forward flow volumes ratio, %	7.7 ± 3.1	9.1 ± 4.2

*: $p<0.05$
**: $p<0.005$
***: $p<0.0001$